Spiral tearing of thin films†‡

Victor Romero,*[ab] Benoît Roman,[b] Eugenio Hamm[a] and Enrique Cerda[a]

Controlling the fracture propagation in a film is an important element in the design of better packaging seals that must resist handling and yet provide a tearing mechanism for easy opening. Here we show that under simple initial setup conditions a divergent tear can be obtained that follows the path of a logarithmic spiral over two decades in length scale. We study the general rules leading to the "spiral growth" of a tear and connect its geometry to the specific material properties of the film.

1 Introduction

Nineteenth century scientists were fascinated by the spiral growth observed in seashells, snails, or the horns of animals.[1,2] It is a clever growth mechanism that preserves the shape by the simple addition of a new material in successive self-similar steps. The classic book of D'Arcy Thompson "On Growth and Form"[2] beautifully explains that this self-similar or "gnomonic" growth is always outlined by a logarithmic spiral. Spiral shapes are not unknown in fracture mechanics. Shrinkage of a sol–gel layer producing a stress field that cracks the film in a complex 3D conical spiral has been reported in the literature.[3,4] The drying of thin layers of precipitates shows millimeter size spiral paths that move inwardly by propagation of a desiccation front.[5,6] However, spiral shapes obtained by tearing are unexpected since fracture trajectories usually converge to minimize the energy concentration generated, for instance, when pulling a flap from a film.[7–11] Thus, convergent tears are a natural outcome when trying to open a sealed package. In contrast, special conditions are needed to observe divergent growth of a tear. Some recent examples of divergent propagation are the tearing produced by pushing a conical tool[12] through a thin aluminum foil, the peeling of coated cylindrical surfaces,[13] and the concertina tearing produced by a blunt object that is forced along a thin elasto-plastic sheet.[8,9,14,31]

Here we report two mechanisms for tearing both leading to a very robust and reproducible divergent path, in brittle materials, commonly used for packaging. We first study fracture propagation obtained by pushing with a blunt object, and,

second by pulling on a flap. The loadings are very different, but in both cases the crack trajectories asymptotically approximate a logarithmic spiral[15] $r = r_0 e^{\theta \cot \phi}$ (in polar coordinates r, θ), with a pole located in a position that depends on the "seed" made to initiate the fracture, and characterized by a constant spiral angle ϕ that is weakly dependent on the material properties of the film. We first show experimental results of spiral crack paths obtained by pushing. We then present a theoretical model and implement a numerical algorithm allowing us to compare theory to experiments. We then turn to the spiral obtained by pulling and perform a similar analysis.

2 Experimental "pushing spiral"

To experimentally study the formation of a spiraling crack, we take a brittle thin sheet (bi-oriented polypropylene, thickness t from 30 to 90 μm), clamped at its edges on a frame (77 × 100 cm²), and make a small (5 mm) straight incision $\mathscr{AB}$ far from the boundaries (see Fig. 1). A blunt object – the "tool" – is placed inside the incision, perpendicular to the sheet. Then we start manually moving the tool horizontally against one of the two lips that define the incision. At a certain load, a crack $\mathscr{T}$ eventually starts to propagate from $\mathscr{B}$ if the pushing point is closer to $\mathscr{B}$ than $\mathscr{A}$. We then keep moving the tool *always pushing on the same lip* of the sheet. We observe that the crack $\mathscr{T}$ describes a curved path that progressively develops into a spiral shape that reaches up to a meter in diameter in about 2.5 turns of the lip [see ESI† where a movie of the process is presented].

During the first $3\pi/2$ degrees of rotation, we need to carefully push the lip in the part closer to the crack to prevent starting a fracture at the other edge of the lip (corner points $\mathscr{B}$ or $\mathscr{A}$, which are subject to stress concentration). But this precaution is no longer necessary for the subsequent propagation of the crack, as we will show below. The remarkable reproducibility of the crack trajectories obtained from this method is shown in Fig. 2 where strikingly similar spirals are obtained from two different trajectories of the pushing object. We also checked that the crack paths are independent of the size and shape of the frame.

[a]*Departamento de Física, Universidad de Santiago, Avenida Ecuador 3493, Estación Central, Santiago, Chile. E-mail: victor.romero@usach.cl*

[b]*PMMH, UMR 7636 CNRS/ESPCI/Paris6/Paris7, 10 rue Vauquelin, 75231 Paris Cedex 5, France*
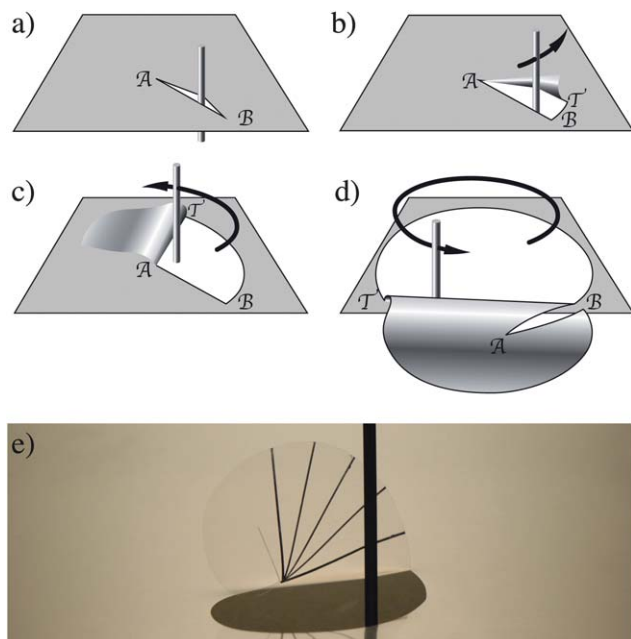
Fig. 1 Illustration of spiral crack propagation by a pushing tool. (a) Initial configuration, (b–d) successive stages of propagation. (e) Experimental configuration at a later stage. Lines diverging from point $\mathcal{B}$ were drawn to guide the eye.
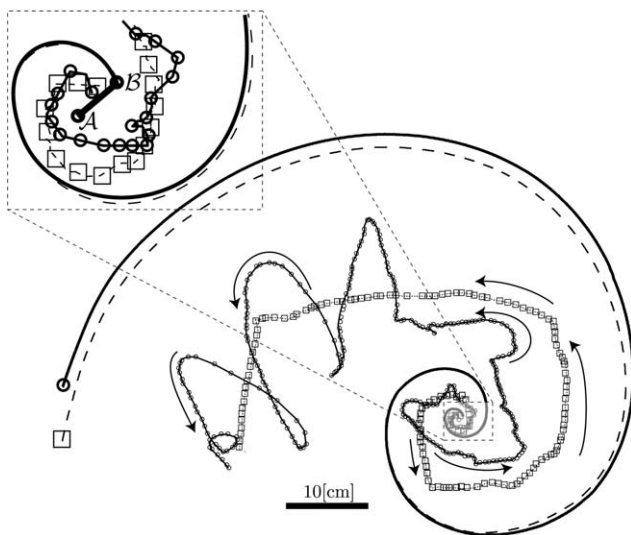
Fig. 2 Scanned crack trajectories for two different experiments. Open circles (squares) show the position of the tool generating the fracture path outlined with the continuous (dotted) line. Density of circles is inversely proportional to the speed of the pushing tool. The arrows show the directions of the tool path for each experiment. Inset: close-up showing the initial cut $\mathcal{AB}$ made to start the crack.

3 Theoretical description

To understand these striking properties and the generation of the spiral, we follow the approach developed in the study of an oscillatory crack path made by a blunt object.[16,19,20] Since resistance to membrane stretching and membrane fracture are linearly proportional to membrane thickness (t), and

membrane bending goes with thickness cubed (t^3), the ease of bending *versus* stretching or fracture increases for thinner films. As a result, thin films primarily respond to loads by bending rather than stretching or fracture, and approximate geometrical solutions can be obtained by studying isometric deformations of the initial flat geometry.[23]

Isometric deformations, however, require boundary conditions compatible with large displacement of the film. This is only possible inside the white in-plane area shown in Fig. 3, where the film easily deforms out-of-plane without stretching. This "soft" region is in geometrical terms the *convex hull* or more precisely, the minimum convex domain that contains the crack path.[15] When placed inside this soft region, the tool only bends the film. But the film is stretched if the tool pushes the borders of the soft region and moves to the dark gray region shown in Fig. 3b. Outside the soft region the main contribution to the elastic energy is the stretching energy located along the edges connecting the tool position with points $\mathcal{A}$ and $\mathcal{T}$. For simplicity we assume in the following that the tool is close to the crack tip $\mathcal{T}$ (see ESI† for more general conditions). In this case the stretching energy is concentrated around the line joining the tool and the crack tip, and must be a function of the two-dimensional Young's modulus $Y = Et$ of the film (where E is the Young's modulus), L is the distance from the tool to the crack tip, and the stretching angle α defined by the vertex at $\mathcal{T}$ of the dark gray region (see Fig. 3). The only combination for the elastic energy compatible with dimensional analysis is $U_E(L, \alpha) = YL^2 u(\alpha)$, where $u(\cdot)$ is a growing function of α that for $\alpha \ll 1$ can be expanded to $u(\alpha) \approx a\alpha^{n+1}$, where a is a dimensionless constant, so that

$$U_E(L, \alpha) = YL^2 u(\alpha) = YL^2 a\alpha^{n+1} \tag{1}$$

The value $n = 4$ is derived by Audoly *et al.*[16] and $n = 3$ by Vermorel *et al.*[12] in contradiction to measurements presented by us elsewhere[17,18] ($n \approx 2.5$, $a \approx 0.0038$). However, the results presented here are fairly insensitive to the precise value of n and the position of the tool along the segment $\mathcal{AT}$.

Knowing the elastic energy, we can compute the force applied to the film by the blunt object through $F = \partial_d U_E$ where d is the normal displacement to the line $\mathcal{AT}$, $d = L \tan \alpha$. For a fixed position of the crack $\delta d = L \sec^2 \alpha\, \delta\alpha \approx L\delta\alpha$, so that the force in terms of our geometrical parameters is $F(L, \alpha) = \partial_\alpha U_E / L$.

For a fixed position of the tool the stretching energy stored in the film can be released by fracture. If point $\mathcal{T}$ moves a distance
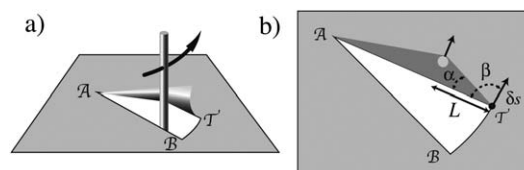
Fig. 3 (a) Detail of the fracture process after Fig. 2c. (b) Geometry of the fracture process. The white zone defines the *convex hull* or the region that is free to move out-of-plane. The dark gray zone is stretched and the resulting elastic energy feeds the crack propagation process.

δs (see Fig. 3), Griffith criterion[21] gives the equilibrium condition $\delta U/\delta s = 0$ (the position of the tool being fixed), where $U = U_E + \gamma t s$ is the total energy of the system, s is the fracture length, and γ is the work of fracture of the film. The variation of the elastic energy when the crack moves a distance δs is $\delta U_E(L, \alpha) = \partial_L U_E \delta L + \partial_\alpha U_E \delta \alpha$ which we combine with the constitutive relationship for the force into

$$\delta U/\delta s = \partial_L U_E \delta L/\delta s + LF\delta\alpha/\delta s + \gamma t = 0 \qquad (2)$$

A crack moving along the direction of propagation β (defined as in Fig. 3) readily implies the geometrical constrains $\delta\alpha = -\sin(\beta - \alpha)\cos\alpha\delta s$ and $\delta L = -\cos\beta\delta s$. Hence, we obtain an expression for $\delta U/\delta s$ as a function of the angles α and β once the constitutive relationships for the energy and the force in eqn (1) are replaced in eqn (2). The maximum energy release criterion $\partial_\beta(\delta U/\delta s) = 0$ (equivalent to minimizing the force[10]) and eqn (2) give two relationships to determine the angles α and β. We obtain

$$\alpha = \left[\frac{\ell_E}{aL(n+1)}\right]^{1/n} \text{ and } \beta = \pi/2 + \frac{n-1}{n+1}\alpha \qquad (3)$$

here $\ell_E = \gamma t/Y$ is similar to an elastocapillary length[22] and is 4 μm for our polymer films. Although this derivation assumed that the tool is much closer to the crack tip than to the other end of the lip (of total length W), in fact these predictions hold even if the tool is placed as far as $4W/5$ from the propagating fracture tip $\mathcal{T}$ (see ESI†).

With $n \approx 2.5$ and $\alpha \ll 1$, we conclude that β is slightly greater than a right angle. Moreover, the angle α depends weakly on the distance L due to the low exponent $1/n \approx 0.4$. Indeed when L is multiplied by a factor 100 (a $L = 2$ mm to $L = 200$ mm range is typical of experiments, see Fig. 2), α is divided by a factor of 6. According to eqn (3), angle α varies[24] from 25° to 4° and angle β changes from 101° to 92°. This gives a total of 9° throughout the generation of a spiral in Fig. 2, with an average value of 96°.

From here on we will therefore assume β to be constant in our analysis, with a value larger than 90° (96° according to our estimates). Propagation is then predicted to take place in an angular direction β, independent of the position of the pushing tool, thus explaining the reproducibility of the experiments shown in Fig. 2.

We now can put together the elements leading to a logarithmic spiral. We identify three stages in the propagation of the crack. First, an initial stage (Fig. 4a) where the crack tip $\mathcal{T}$ propagates in a direction with a constant angle β with respect to the radius $\mathcal{AT}$. This is a sufficient condition to have a logarithmic spiral centered at point $\mathcal{A}$ with a pitch due to an angle $\phi = \pi - \beta$. Second, after half a turn the crack reaches point $\mathcal{C}$ and transforms the morphology of the convex hull (see Fig. 4a and b). The soft region is delimited by the line $\mathcal{BT}$, so that the crack follows another logarithmic spiral with the same angle $\phi = \pi - \beta$, but now centered at point $\mathcal{B}$. The crack trajectory is smooth across point $\mathcal{C}$ because the tangent keeps the same angle β with lines $\mathcal{AT}$ and $\mathcal{BT}$. However, the jump from $\mathcal{A}$ to $\mathcal{B}$ in the position of the pole implies a discontinuity in the radius of curvature R since for a logarithmic spiral[15] $R = r/\sin\phi$. Third,
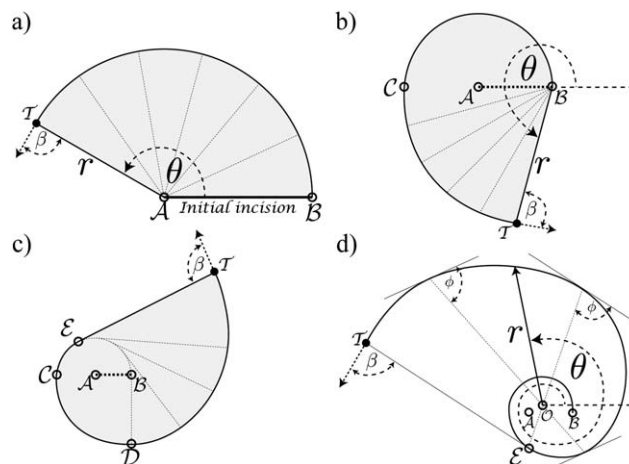
Fig. 4 The morphology of the soft zone defines three different stages in the evolution of the spiral, in light gray we show the soft zone for each stage. (a) First stage: the spiral grows with a center point at $\mathcal{A}$. (b) Second stage: the pole of the spiral is now point $\mathcal{B}$. (c) Third stage: the path grows by successive increments applied to the line $\mathcal{ET}$. (d) The figure shows the geometrical construction to obtain the asymptotic center of the pole in our experiments (see text).

after roughly another quarter turn the convex hull is no longer limited by the line $\mathcal{BT}$. At position $\mathcal{D}$ (see Fig. 4c), the construction point $\mathcal{E}$ defines the convex hull and moves tangentially to the trail left by the crack path to exhaust pure bending deformations. The crack path now develops around itself in a self-similar way while the tear grows by successive increments applied to the segment[25] $\mathcal{ET}$ shown in Fig. 4c.

4 Numerical model and experiments

We use a numerical algorithm to generate the spiral path predicted by eqn (3). At each step the model calculates the convex hull and then the direction of the propagation of the fracture. Fig. 4c illustrates the procedure to obtain the direction of propagation once the position of the crack in $\mathcal{T}$ is given. The determination of the convex hull defines point $\mathcal{E}$ and the unitary vector t (dotted arrow vector in Fig. 4) making an angle β with the line $\mathcal{ET}$. The fracture moves a length δs along t and a new position of point $\mathcal{T}$ is computed. The current position of point $\mathcal{T}$ redefines the morphology of the convex hull and the process must be repeated again. The numerical curve obtained from the algorithm can be studied locally to know how similar the curve is to a logarithmic spiral. We follow the method suggested in D'Arcy Thompson's book[2] based on local geometrical properties of the curve. To obtain the instantaneous value of the spiral angle[2,15] we calculate the rate dR/ds at which the radius of curvature varies along the crack path. This quantity has the value $\cot\phi$ for a perfect logarithmic spiral. Once the local value of $\cot\phi$ is calculated in two neighboring points, we compute the instantaneous position of the pole by intersecting the lines making an angle ϕ with the respective tangents at those points. Finally, the determination of the pole position gives the distance r and polar angle θ (see Fig. 4d). The inset in Fig. 5a shows the instantaneous position of the pole obtained by

this numerical procedure. The pole is at point $\mathscr{A}$ and point $\mathscr{B}$ in the first and second stages, respectively, and then moves progressively towards a fixed point $\mathscr{O}$, an indication that the spiral is asymptotically reaching a logarithmic spiral.

The semilog plot in Fig. 5a gives the numerical function $r = r(\theta)$. It shows how the path crack develops into a logarithmic spiral since the slope of the figure represents the local value of $\cot \phi$. The slope is constant and equal to $\cot(\pi - \beta)$ in the interval[26] $0 < \theta < 3\pi/2$, as was expected from our analysis for the first and second stages. More interestingly, the slope also approximates a constant number for large values of θ. We can easily understand the geometry of the asymptotic path from studying the convex hull defined by a logarithmic spiral. We show in ESI† that a perfect logarithmic spiral of angle ϕ has an angle β given by the transcendental relationship (see ESI† for derivation of this property).

$$\sin \phi e^{-\cot \phi(2\pi - \beta)} - \sin(\beta + \phi) = 0 \qquad (4)$$

A numerical solution yields, for instance, $\cot \phi \approx 0.27$ for $\beta = \pi/2$.

To test the model, we study the geometrical shapes of the tears obtained in our experiments. The pole was experimentally fixed at points $\mathscr{A}$ and $\mathscr{B}$ in the first and second stages, respectively, and a global method was used to obtain the asymptotic position of the pole when the logarithmic spiral is fully developed. Fig. 4d shows the experimental procedure to obtain the pole position. Two parallel tangents to a logarithmic spiral define a line where the pole $\mathscr{O}$ must lie. The pole position is obtained by intersecting two of these lines. In the dimensionless coordinates of Fig. 5a (inset), we obtain an approximate position [0.4, 0.2] for the pole in our experiments which is consistent with our numerical model that gives the asymptotic value [0.4, 0.1]. Once the position of the pole is established, it is straightforward to measure from our samples the distance $\mathscr{O}\mathscr{T}$ and the angle of rotation θ to obtain the experimental curve $r = r(\theta)$.

The local values of β can also be extracted from *post mortem* analysis of experimental crack path. Fig. 5b shows that β has regular oscillations of period π around a constant value $\langle \beta \rangle = 92.3° \pm 9°$ (the error range represents the amplitude of oscillations). The average value is consistent, but slightly lower than our prediction $\beta = 96°$ (see Section 3). Oscillations represent variations in the work of fracture due to anisotropy, that are not considered in eqn (2). They can be cancelled out in the average by doing a pair of experiments with initial starting cuts at perpendicular directions or by taking several oscillations along the same experiment (see Fig. 5b). We note that the amplitude of oscillation (18° peak to peak) is larger than the overall variation (estimated 9°) given by eqn (3) when L changes in two orders of magnitude.

Fig. 5a shows in a semilog plot the radius of the spiral as a function of the angle of rotation in our experiments. The crack path behaves roughly as a logarithmic spiral with an experimental slope $\cot \phi = 0.29 \pm 0.01$ which is consistent with that given by eqn (4), $\cot \phi = 0.29$, if the value $\beta = 92.3°$ is used. We also observe oscillations around the exponential growth that are due to material anisotropy, resulting in local variations of the angle β observed in Fig. 5b.

5 The starting seed

We discuss the conditions to obtain a spiral growth of a tear. Our initial seed, line $\mathscr{A}\mathscr{B}$, to propagate the crack was dictated by simplicity. However, it has some disadvantages. The film contains two competing cracks along the first and second stages and care must be taken to avoid the propagation of the crack at the position of the pole. In mathematical terms, the convex hull has a perimeter with two discontinuities for the tangent in the first two stages. At these discontinuities, the tangent defines an exterior angle[28] $\mathscr{X}$ $(= \beta$ in Fig. 4c) that accounts for the change of curvature $\int ds \, R^{-1} = \mathscr{X}$ at the discontinuity (here R is the radius of curvature of the convex hull). Thus, the presence of an exterior angle implies a high value of the curvature and stress concentration at the position of the moving crack $\mathscr{T}$ and the pole.

The same rules followed by the crack propagation contain the remedy for the stress concentration at the pole. We observe that in the beginning of the third stage the second crack disappears when point $\mathscr{T}$ passes point $\mathscr{D}$ (see Fig. 4c). The convex hull perimeter now has a continuous tangent near the subsequent point $\mathscr{E}$ which smoothens the curvature. To prevent the presence of a second crack in the first and second stages, we

Fig. 5 (a) Semilog plot of the curve $r = r(\theta)$ in units of the initial distance $r_0 = \mathscr{A}\mathscr{B}$. The black line is obtained from our numerical spiral for $\beta = 92.3°$. The circles represent the experimental measurements of two spirals started with cuts in two perpendicular orientations. The instantaneous pole in our experiments is chosen as $\mathscr{A}$ for $\theta < \pi$, $\mathscr{B}$ for $\pi < \theta < 3\pi/2$, and the asymptotic value of $\mathscr{O}$ for $3\pi < \theta < 6\pi$. Inset: the instantaneous position of the pole obtained from the numerical model for $\beta = 92.3°$. The pole moves progressively to the asymptotic position $\mathscr{O} \approx [0.4, 0.1]$ in dimensionless units. The successive jumps in the position of the pole reflects a discontinuity in the curve $r = r(\theta)$ and its curvature. (b) Fracture angle β measured as a function of the polar angle θ for the same two spirals shown in (a).

can design an initial seed with a convex hull outlined by a perimeter with one exterior angle. This angle must be conveniently chosen to avoid shedding a new crack when propagating the fracture. The obvious candidate is an initial cut having a convex hull with the same shape of the spiral (region $\mathscr{CDTE}$ in Fig. 4c). However, this does not exhaust the possible seeds. We conjecture that *any cut with a convex hull containing only one point of discontinuity in the tangent which defines an exterior angle $\mathscr{X} \leq \beta$ would lead to the same result.*

6 Pulling spirals

Spiral crack paths are not restricted to the situation where a tool is pushed against the sheet. Instead of pushing the lip $\mathscr{ET}$ in Fig. 4c, the tear can be *pulled* upwards to propagate the crack, as shown in Fig. 6. To systematically study spiral propagation by pulling, we replace the initial straight incision made for the pushing case by a circle cut with a curved notch $\mathscr{AB}$ that follows the recipe given in the last section. The cut $\mathscr{AB}$ is conveniently prepared to have a convex hull with no discontinuity at point $\mathscr{A}$ and an exterior angle β at point $\mathscr{B}$. By pulling upwards the flap left by the notch, the crack at $\mathscr{B}$ starts propagating along a spiral path (see ESI† where a movie of the process is presented).

Because of the very low bending rigidity, all the region where the sheet can move out-of-plane does so (see Fig. 6). We have seen earlier that this region is the convex hull of the cut. As a result, the operator effectively pulls on a fold which is a segment starting on the crack tip $\mathscr{T}$ and reaching tangentially the previous cut at point $\mathscr{E}$. This fold shares exactly the same geometry with the lip on which the tool was pushing in previous sections. However, the loading is of course different from the pushing spiral. The fracture is now mediated by a fold connecting the flap with the film where bending and stretching energy is focused. In a rather similar case of a torn flap strongly adhering to a substrate,[10,13] fracture propagates with an angle β lower than $\pi/2$. In the geometry studied here, we can only

provide a rough estimate of angle $\beta = \pi/2 - 4\sqrt{l_B/L}$ based on the assumption that the fold takes a cylindrical shape. Here L is the total length of the fold, and $\ell_B = B/\gamma t$ is a new length scale in the problem, involving work of fracture and bending rigidity B. We again notice a weak dependence of the inward angle $\pi/2 - \beta$ of propagation (inverse square root) with the width of the fold L. Moreover, in our experiments this angle is very small (on the order of 4 degrees for typical a value of $L = 10$ cm) because $\ell_B \sim 30$ μm. In fact $\ell_B \to 0$ when $t \to 0$ (compare with ℓ_E that remains constant in this limit), so that propagation tends to be perpendicular to the fold in this infinitely thin sheet limit.[29] We will therefore again assume that β is a constant in a first approximation. We then expect a self-developing logarithmic spiral very similar to the previous case.

Proceeding in the same way as for the spiral obtained by pushing, we determine the pole of the spiral obtained by pulling, and thereafter we measure the distance $\mathscr{OT}$, the angle of rotation θ, and the local angles α and β. In Fig. 7a we plot $r = r(\theta)$. Fig. 7b shows that β has regular oscillations of period π around a constant value $\langle \beta \rangle = 86.9° \pm 9.0°$. Here the error includes the amplitude of the observed oscillations. The fact that $\beta < \pi/2$ does not prevent the spiral to be divergent though. The semilog plot of Fig. 7a shows that the crack path behaves in average as a logarithmic spiral with an experimental slope cot $\phi = 0.24 \pm 0.01$ which agrees with the estimation given by eqn (4) cot $\phi = 0.25$. This lower pitch of the spiral is consistent with propagation with a predicted angle β slightly lower than $\pi/2$. Here again anisotropy of the material results in a periodic effect on the direction of propagation.
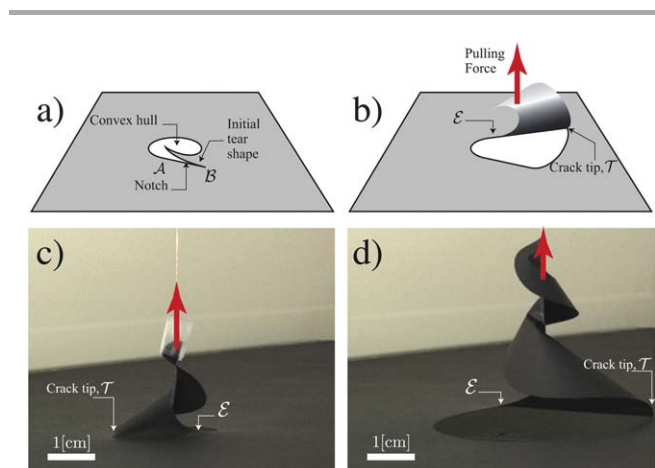
Fig. 6 Spiral crack obtained by pulling on a flap of material. (a) Initial stage at which a notch is cut tangent to a circular hole in the sheet; (b) initial pulling leads to a crack path; (c) and (d), later stages of crack propagation. Note the way in which the released strip twists along the pushing direction forming a pine tree structure.
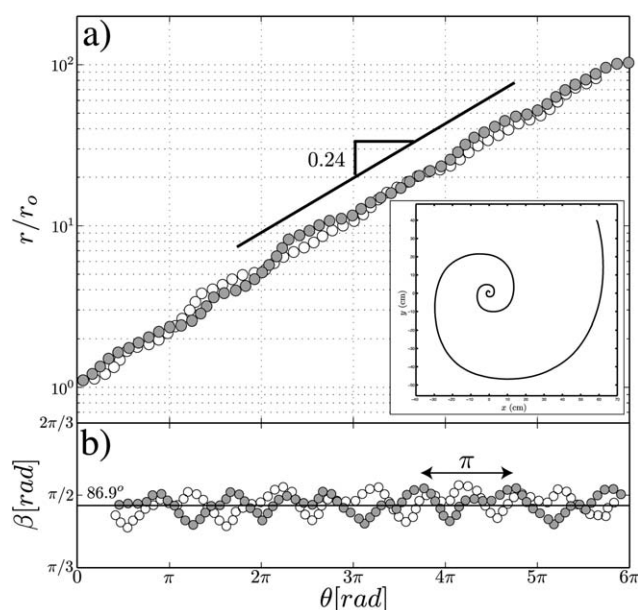
Fig. 7 Experimental pulled spiral (inset: scanned fracture trajectory). Measurement of the radius of the spiral as a function of the rotation angle for two spirals. Here r_0 corresponds to the minimum measured radius of the spiral obtained by using our experimental method explained in Section 4. It corresponds to the distance from the spiral pole to point $\mathscr{B}$, typically 0.7 cm. The figure at the bottom represents measurements of propagation angle β exhibiting oscillations due to anisotropy around an average value slightly lower than $\pi/2$.

Although there is stress concentration at points $\mathscr{T}$ and $\mathscr{E}$, the softening of the curvature at point $\mathscr{E}$ acts as a crack stopping mechanism that prevents this possibility. Thus, the tear will grow by adding new increments defined by the characteristic angle β of the specific configuration. In general, we expect that other mechanisms of crack propagation may change the value of β, but keeping the asymptotic spiral shape of the tear. This robustness is further explained by the fact that for any possible direction of propagation of the crack, $0 < \beta < \pi$, eqn (4) gives always a divergent path ($0 < \phi < \pi/2$). For instance, a film adhered to a substrate and pulled along the line $\mathscr{E}\mathscr{T}$ will have an angle β related to the material properties of the film and substrate as derived by Hamm et al.[10]

The authors have presented a patent[30] in the context of the design of efficient opening mechanisms in packaging of goods. The patent takes advantage of two basic ideas put forward in Sections 5 and 6: (1) a seed is required to allow only one crack to move safely, without shedding more cracks, when tearing a packaging film, and (2) a spiral propagation is obtained no matter what mechanism of tearing is used (pulling or pushing). A spiral mode of tearing can be naturally applied to the opening of a wrapper, in contrast to convergent cracks that require more than one pushing or pulling operation for complete unwrapping.

7 Conclusions

We have observed and theoretically described self-developing logarithmic spiral crack paths in thin elastic and brittle sheets, for two different loading conditions (pushing and pulling). In both cases fracture propagation obeys the same geometrical construction. A soft zone, the convex hull, bends away, and fracture propagates with a constant angle with respect to the limiting lip of material connecting the flap with the film. The crack propagation adds more area to the convex hull in a self-similar manner producing a spiral tearing. The asymptotic logarithmic spiral path is independent of the initial shape of the soft zone. However, the starting seed must be designed with a convenient shape in order to allow a single crack to propagate.

The process is very robust. Indeed when the size L of the lip satisfies $L \gg \ell_E$ (pushing) or $L \gg \ell_B$ (pulling) the process does not depend on the material properties and becomes purely geometrical.[29] Boundary conditions, particularly the size of the frame that holds the sheet, are not determinant. This is consistent with our assumption that all elastic energy focuses in the vicinity of the line $\mathscr{T}\mathscr{E}$, which leads to satisfactory predictions for the values of α and β, either in the pushing or the pulling case.

The generality of the mechanism can be further illustrated by applying it to tear thin metal films. Indeed, if the fracture process zone is small (low work of fracture[27]), our geometrical description in terms of the convex hull still holds. Even if plasticity also takes place in areas away from the crack but near the fold, fracture propagation is still strongly oriented by geometry.[7–9,14] Thus, we expect spiral crack propagation to be observed in different materials (brittle or ductile) and configurations when material properties and the initial flap design avoid the nucleation of a second crack while tearing.

Notes and references

1 T. A. Cook, *The Curves of Life*, Dover, New York, 1979.
2 D. W. Thompson, *On Growth and Form*, Dover, New York, 1992.
3 D. Hull, *Fractography*, Cambridge University Press, Cambridge, 1999.
4 M. Sendova and K. Willis, *Appl. Phys. A: Mater. Sci. Process.*, 2003, **76**, 957.
5 Z. Néda, K.-t. Leung, L. Jozsa and M. Ravasz, *Phys. Rev. Lett.*, 2002, **88**, 9.
6 V. Lazarus and L. Pauchard, *Soft Matter*, 2011, **7**, 2552.
7 T. Wierzbicki, K. A. Trauth and A. G. Atkins, *J. Appl. Mech.*, 1998, **65**, 991.
8 A. G. Atkins, *Endeavour*, 1995, **19**, 1.
9 A. G. Atkins, Science & Public Affairs, *Autumn*, 1994, **19**.
10 E. Hamm, P. Reis, M. Leblanc, B. Roman and E. Cerda, *Nat. Mater.*, 2008, **7**, 386.
11 E. Bayart, A. Boudaoud and M. Adda-Bedia, *Phys. Rev. Lett.*, 2011, **106**, 19.
12 R. Vermorel, *et al.*, *Phys. Rev. Lett.*, 2010, **104**, 175502.
13 O. Kruglova, F. Brau, D. Villers and P. Damman, *Phys. Rev. Lett.*, 2011, **107**, 164303.
14 T. Tallinen and L. Mahadevan, *Phys. Rev. Lett.*, 2011, **107**, 245502.
15 H. W. Guggenheimer, *Differential Geometry*, Dover, New York, 1977.
16 B. Audoly, P. M. Reis and B. Roman, *Phys. Rev. Lett.*, 2005, **95**, 025502.
17 V. Romero, Ph.D. thesis, Université Pierre et Marie Curie and Universidad de Santiago, 2010.
18 V. Romero, B. Roman, E. Hamm and E. Cerda, unpublished.
19 B. Roman, P. M. Reis, B. Audoly, S. De Villiers, V. Viguié and D. Vallet, *C. R. Mec.*, 2003, **331**, 811.
20 P. M. Reis, A. Kumar, M. D. Shattuck and B. Roman, *Europhys. Lett.*, 2008, **82**(6), 64002.
21 B. Lawn, *Fracture of Brittle Solids*, Cambridge University Press, 2nd edn, Cambridge, 2004.
22 B. Roman and J. Bico, Elasto-capillarity: deforming an elastic structure with a liquid droplet, *J. Phys.: Condens. Matter*, 2010, **22**(49), 493101.
23 T. A. Witten, *Rev. Mod. Phys.*, 2007, **79**, 643.
24 We use $n \approx 2.5$, $a = 0.0038$, and $\ell_E = 4$ μm in eqn (3) and obtain $\alpha = 25°$, 4° and $\beta = 101°$, 92° for $L = 2200$ mm respectively.
25 Incidentally this way of growth has been reported in D'Arcy Thompson's book [ref. 2] and references within to explain the spiral growth of the structure covering the aperture (Opercula) in Nerita shells.

26 The exact value of the upper limit for this region is $\theta = 3\pi/2 - (\beta - \pi/2) \approx 267.7°$ since the crack started at an angle β at point $\mathscr{B}$.

27 Work of fracture is proportional to thickness ($\gamma \sim t$) in thin metal films [ref. 14].

28 D. J. Struik, *Lectures on Classical Differential Geometry*, Dover, New York, 1988.

29 B. Roman, Fracture path in brittle thin sheets : a unifying review on tearing, *Int. J. Fract.*, 2013, in press.

30 V. Romero, B. Roman, E. Hamm and E. Cerda, Film Mince D'emballage à amorce de dchirure, European Patent no 10805796, 9–2308, 2010.

31 E. Villermaux and N. Vandenberghe, *Soft Matter*, 2013, DOI: 10.1039/C3SM50789K.